

# Computational Analysis of Biomedical Data

Eleni Zacharia\*

National and Kapodistrian University of Athens  
Department of Informatics and Telecommunications  
zacharia@di.uoa.gr

**Abstract.** In the present PhD thesis, original methods of computational analysis are put forward, which focus on image analysis and processing. The proposed methods are applied in biomedical images, such as cDNA microarray images as well as 2D gels images that are obtained from two-dimensional electrophoresis of proteins. They exploit the intensity information of the images and convert basic problems of analysis and processing, such as the determination of grid structure (gridding) and spot segmentation, to optimization problems which are subsequently solved using the methodology of genetic algorithms. The proposed methods of gridding and spot-segmentation have been applied to synthetic images as well as to real ones. Their application results have showed that the proposed methods achieve higher accuracy in comparison to various well-known and broadly used techniques.

**Keywords:** Image Analysis, Segmentation, Genetic Algorithms, Optimization Problem, Biomedical data, Microarrays, 2D gels.

## 1 Introduction

In terms of research, for the past ten years the analysis of biomedical images – such as cDNA microarray images as well as 2D gels images that are obtained from two-dimensional electrophoresis of proteins – has been at the forefront of biomedical science. Indeed, these images are being increasingly applied in numerous fields of biomedical research such as cancer research, pharmaceutical research, toxicological research, infectious disease diagnosis and treatment, and agricultural development. The reason behind their broad use and success can be found in their main revolutionary feature: the ability to analyze the expression levels of thousands of genes over different samples simultaneously.

The end product of either the microarray experiment or the two-dimensional electrophoresis of proteins is a high resolution digital image, containing thousands of spots, the intensities of which are proportional to the expression levels of specific genes. Consequently, image analysis is necessary for the detection of spots' boundaries and the calculation of their intensity.

The process of analyzing a microarray image can be divided into three main phases namely: Gridding, Spot-Segmentation and Spot-Intensity Extraction. During the 1<sup>st</sup>

---

\* Dissertation Advisor: Dimitris Maroulis, Associate Professor

phase, the microarray image is segmented into numerous compartments, each containing one individual spot and background. During the 2<sup>nd</sup> phase each compartment is individually segmented into a spot area and a background area, while during the 3<sup>rd</sup> phase the brightness of each spot is calculated. The expression-levels of the genes in these spots result from their individual brightness. The analysis of the 2D gels includes only the latter two phases.

There is a considerable number of software systems and techniques that have been developed and proposed to date, in order to analyze the aforementioned images. However, the currently available software packages have several limitations not least because of the poor quality of microarray images. Indeed, these images are contaminated with noise, and artifacts. Moreover, real spots vary significantly from the ideal ones; they are not always circular in shape and their intensity is not always high enough to be clearly visible. Human intervention is therefore necessary either for the initialization of their input parameters, or for the rectification of their incorrect results. Consequently, the analysis and processing of the aforementioned images becomes on the one hand time-consuming, since the users have to choose the appropriate values for their input parameters and rectify their results, and on the other hand subjective, since the users initialize and correct the software programs in an individual manner. This subjectivity can in turn affect the biological results. As a matter of fact, the biological results often differ from the real ones.

In this chapter, accurate algorithms are presented that implement (i) the automatic gridding phase for microarray images and (ii) the spot-segmentation phase for both the microarray images and 2D gels. All these algorithms are based on the optimization technique of evolutionary algorithms and of genetic algorithms in particular. Consequently, prior to describing these methods, a brief introduction to the evolutionary genetic-algorithms technique is apposed. It should be noted that various aspects of this research have been published or submitted in two peer-reviewed international journals [1][2], in a chapter of a book [3], in the peer-reviewed proceedings of six international conferences [4]-[9], and in the peer-reviewed proceedings of one national conference [10]. The remainder of this chapter is organized in six sections: In section 2 a brief description of the evolutionary genetic-algorithms optimization technique is provided. In Sections 3, 4 and 5 three advanced evolutionary genetic algorithms are presented which implement the automatic gridding phase for microarray images and the spot-segmentation phase for both microarray images and 2D gels. Section 6 illustrates the experimental results, while in section 7 conclusions are apposed.

## **2 Evolutionary Genetic-Algorithms Optimization Technique**

Genetic-Algorithm (GA) is a powerful optimization search methodology based on the principles of natural selection and evolution. A conventional GA [11] begins its search by constructing a finite number of potential solutions encoded as alpha-numerical sequences called chromosomes. These chromosomes, which constitute an initial population  $Pop_1$ , are evaluated using a fitness function. Subsequently, the population  $Pop_1$  evolves into a new population  $Pop_2$  using the following three genetic

operators: reproduction, crossover, and mutation. This evolutionary cycle of a current population  $Pop_n$  to its next  $Pop_{n+1}$  (where  $n$  stands for the consecutive number of populations) continues until a specific termination criterion is satisfied.

The evolutionary genetic algorithms used in the gridding and the spot-segmenting phases enclose the same evolutionary cycle and termination criteria. More precisely, a new population  $Pop_{n+1}$  is created from the current  $Pop_n$  by applying the following stages: (i) Reproduction stage:  $P_r\%$  of the best chromosomes of the current population  $Pop_n$  are carried over to the new population  $Pop_{n+1}$ , and (ii) Crossover-Mutation stage: The chromosomes needed to complete the new population  $Pop_{n+1}$  are produced through iterations; four chromosomes of the population  $Pop_n$  are selected using the tournament selection method [12]. These chromosomes are subsequently subjected to the joint application of the BLX-a [13] and the dynamic heuristic crossover [13] operator, according to a  $P_c\%$  probability and then to the wavelet mutation operator [14], according to a  $P_m\%$  probability. The best two of the four resulting chromosomes advance to the new population  $Pop_{n+1}$ . Moreover, the genetic algorithms are executed up to a maximum number of populations  $G_{Max}$ , or up to a maximum number of populations  $G_{Fit}$  for which the best fitness value has remained unchanged.

## 2 Gridding of Microarray Images

The proposed approach to the gridding of microarray images is divided into the following two main stages: (i) The microarray image is segmented into blocks, by determining (drawing) a set  $S_B$  of line-segments whose members are the line-segments constituting the borders of adjacent blocks (Stage I), and (ii) Each block (from Stage I) is segmented into single-spot compartments, by determining (drawing) a set  $S_S$  of line-segments whose members are the line-segments constituting the borders between adjacent spots (Stage II).

Let  $G$  be a microarray image or block. Each of the  $S_B$  or  $S_S$  sets can be divided into the following two sub-sets: i) a sub-set  $S_V$  of line-segments whose members are defined by the two vertical sides of  $G$ , and ii) a sub-set  $S_H$  of line-segments whose members are defined by the two horizontal sides of  $G$ .

### 2.1 The proposed Genetic Algorithm

The determination of line-segments which are included in either the  $S_V$  or the  $S_H$  sub-sets can be viewed as an optimization problem which is tackled by using the proposed Genetic Algorithm which determines the exact values of the variables of all the line-segments included in both subsets, one sub-set at a time.

### 2.1.1 Chromosome Representation

Each chromosome  $m$  of the proposed Genetic Algorithm represents all line-segments  $L_i, i=1, \dots, N(m)$  belonging to the  $S_V$  or  $S_H$  sub-set, where  $N(m)$  is the number of the line-segments belonging to the respective sub-set. Therefore, it has been encoded as a string of real values containing two segments. The first one encodes the exact values of the parameters of one line-segment, while the second one encodes the distance  $d$  between two adjacent line-segments. In the case when the Genetic Algorithm searches for the exact values of the variables of the optimal line-segments belonging to the  $S_V$  sub-set, its chromosome will encode the exact values of the parameters of  $line_{V1}$  and  $d_V$  (Fig. 1). In the case when the Genetic Algorithm searches for the exact values of the variables of the optimal line-segments belonging to the  $S_H$  sub-set its chromosome will encode the exact values of the parameters of  $line_{H1}$  and  $d_H$  (Fig. 1).

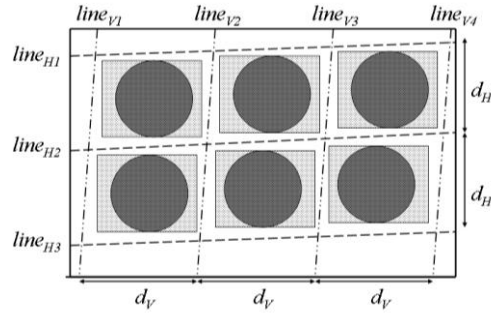


Fig. 1. Line-segments constituting the grid structure in a microarray image or block.

### 2.1.2 Chromosome Evaluation

A line-segment which is part of the grid is located in an area empty of spots. The pixels of this area are part of the background and their intensities are generally lower than the intensities of the pixels constituting spots. As a result, we define the probability  $P(L_i)$  of a line-segment  $L_i$  to be part of the grid by the following equation:

$$P(L_i) = f_B^{R_{L_i}}(L_i) - f_S^{R_{L_i}}(L_i) \quad (1)$$

$R_{L_i}$  denotes the region of  $G$  which contains those pixels whose distance from the line-segment  $L_i$  is less than a margin  $w$ . The real-valued function  $f_B^{R_{L_i}}(L_i)$  expresses the percentage of pixels of the region  $R_{L_i}$  whose intensity is lower than a value  $I_B$ , while the real-valued function  $f_S^{R_{L_i}}(L_i)$  expresses the percentage of pixels of the region  $R_{L_i}$  whose intensity is higher than a value  $I_B$ .  $I_B$  is an intensity value which is defined as the value which is present in most pixels of  $G$ . Any pixel below this intensity value  $I_B$  belongs to the background.

The fitness function  $F(m)$  of a chromosome  $m$  that encodes a possible solution to the particular optimization problem is defined by the following equation:

$$F(m) = \begin{cases} S_p(m) \cdot N(m), & \text{if } f_{LS}(m) \leq f_{Max} \\ S_p(m), & \text{otherwise} \end{cases} \quad (2)$$

The real-valued function  $S_p(m)$  denotes a total sum of the probabilities  $P(L_i)$  of the line-segments  $L_i$ ,  $i=1, \dots, N(m)$ , that are represented by the chromosome  $m$ , and have a high probability  $P(L_i)$  to be part of the grid. The real-valued function  $f_{LS}(m)$  denotes the percentage of the line-segments  $L_i$ ,  $i=1, \dots, N(m)$ , that are represented by the chromosome  $m$ , and have a low probability  $P(L_i)$  to be part of the grid. A high probability  $P(L_i)$  is the one which is higher than a threshold  $P_{MAX}$ , while a low one is the one which is lower than a threshold  $P_{LOW}$ , where  $P_{LOW} < P_{MAX}$ .  $N(m)$  denotes the total number of the line-segments  $L_i$  which are represented by the chromosome  $m$ .

## 2.2 The refinement procedure

It is worth pointing out that due to the alignment of blocks inside the microarray image and the arrangement of spots inside the blocks, the line-segments – having the same direction and constituting the borders of blocks (or spots) – are ideally equidistant. However, this observation may not come true when rotations, misalignments and local deformations of the ideal rectangular grid exist. As a result, the determined line-segments may slightly vary from the optimal ones.

In order to tackle this problem, each line-segment  $L_i$  belonging to the  $S_V$  or  $S_H$  sub-sets is replaced with a new one,  $L_i'$ , under the following two conditions: i) the line-segment  $L_i'$  is located inside the region  $R_{L_i}$  of  $G$ , 2) the probability  $P(L_i')$ , of the line-segment  $L_i'$ , to be part of the grid, is higher than the equivalent probability of  $L_i$  ( $P(L_i)$ ), by more than a threshold  $T_p$ . An example of the refinement procedure is depicted in Fig. 2.

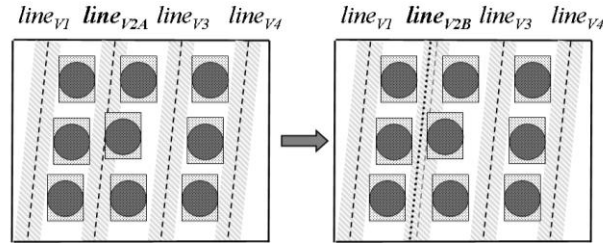


Fig. 2. The line-segment  $line_{v2A}$  is replaced with the line-segment  $line_{v2B}$ . The high-lighted areas on either sides of the line-segments denote the regions  $R_{L_i}$ .

## 3 Spot Segmenting in microarray images

According to Kim et al [15], microarray spots can be classified into three categories according to their shape: peak-shaped, volcano-shaped, and doughnut-shaped spots (Fig.3). Based on the aforementioned remark, our proposed segmentation method is conducted into two stages: (i) The morphological spot shape is represented by a spot-model, and (ii) The spot contour is depicted in the image plane by drawing the contour of its spot-model.

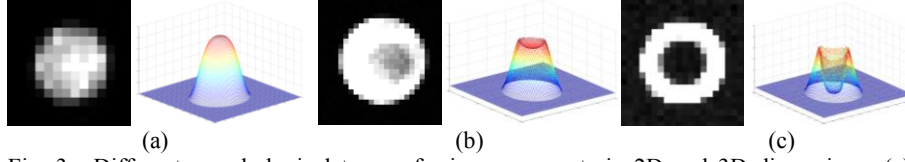


Fig. 3. Different morphological types of microarray spots in 2D and 3D dimensions: (a) a peak-shaped spot, (b) a volcano-shaped spot, (c) a doughnut-shaped spot.

### 3.1 Morphological Models for a Microarray Spot and its Compartment

All the aforementioned spots categories can be represented using: i) a 3D-curve representing the main-body  $S_{MB}$  of the spot-model, and ii) a 3D-curve representing the inner-dip  $S_{ID}$  of the spot-model. Both the main-body and the inner-dip 3D curves resemble the 3D Gaussian or plateau curve. Moreover, their orientation is opposite; the base of the main-body of the spot-model is down and its peak is up, while the base of the inner-dip of the spot-model is up and its peak is down (Fig.4).

The spot-model  $S_{MODEL}(x,y)$  is constructed by combining the  $S_{MB}(x,y)$  and  $S_{ID}(x,y)$  3D-curves as the following equation indicates:

$$S_{MODEL}(x, y) = \text{Min} [S_{MB}(x, y), S_{ID}(x, y)] . \quad (3)$$

A graphical explanation of eq. 3 is depicted in Fig. 4. The resulting total-models (grey areas) depend on the 3D curves of their corresponding  $S_{MB}$  and  $S_{ID}$  components. More precisely, in the case of the distance between the  $S_{MB}$  and  $S_{ID}$  centers being large, the resulting total-model resembles a peak-shaped spot (Fig.4a). In the case of the distance between the  $S_{MB}$  and  $S_{ID}$  centers being small, the resulting total-model resembles a volcano-shaped spot (Fig.4b) or a doughnut-shaped spot (Fig.4c), according to the height of the  $S_{ID}$  3D curve.

Likewise, the morphological compartment-model can be defined as:

$$I_{MODEL}(x, y) = \text{Max} B_{AV}, S_{MODEL}(x, y) \quad (4)$$

where  $B_{AV}$  denotes the average background intensity of the compartment-model and it corresponds to a threshold of the lowest values of the  $S_{MODEL}(x,y)$ . Pixels whose values are lower than  $B_{AV}$  belong to the background and their values are set equal to  $B_{AV}$ . A graphical explanation of eq. 4 for a volcano-shaped spot is depicted in Fig. 5.

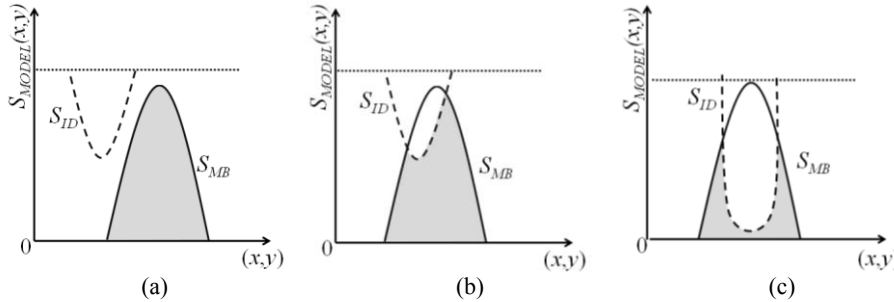


Fig. 4.  $S_{MB}$  and  $S_{ID}$  components of the morphological models of: (a) a peak-shaped spot, (b) a volcano-shaped spot, (c) a doughnut-shaped spot. The total morphological models are the grey areas.

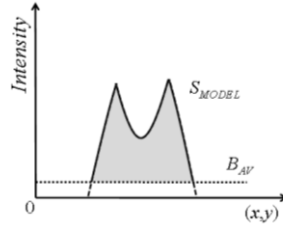


Fig. 5. Morphological model for a compartment containing a volcano-shaped spot.

### 3.2 Optimum Spot-Model Representation and Definition of Real-Spot Contour

A genetic algorithm determines the compartment-model which optimally represents the real-one. In order to achieve this, it searches for the optimal values of the parameters of the morphological compartment-model defined by eq. (4).

#### 3.2.1 Chromosome Representation

Each chromosome  $m$  represents a morphological compartment-model  $I_{MODEL}^m$ . Consequently, it is encoded as a numerical sequence consisting of three segments: The first segment encodes the value of the average background intensity  $B_{AV}^m$  of the compartment-model. The second segment encodes the values of the variables of the main-body  $S_{MB}^m$ , while the third segment encodes the values of the variables of the inner-dip  $S_{ID}^m$  of the spot-model  $S_{MODEL}^m$ .

#### 3.2.2 Chromosome Evaluation

The higher the resemblance of the morphological compartment-model  $I_{MODEL}^m$  (represented by the chromosome  $m$ ) to the real-compartment  $I_{REAL}$  is, the higher the value of the fitness function of a chromosome  $m$  becomes. As a result, the genetic algorithm can progressively assign – from left to right – a higher fitness value to the chromosomes representing the compartment-models in Fig. 6.

## 4 Spot Segmenting in 2D gel images

The methodology which was developed resembles the aforementioned one. The segmentation process is based on the possibility of the diffusion model to represent the three-dimensional morphology of the spots and is tackled by using genetic algorithms. However, in the present approach the original genetic algorithm takes under consideration possible overlaps of adjacent spots and determines in parallel the parameters of multiple diffusion models that optimally represent them. The detection and segmentation of the overlapping spots is conducted by the superposition of two or

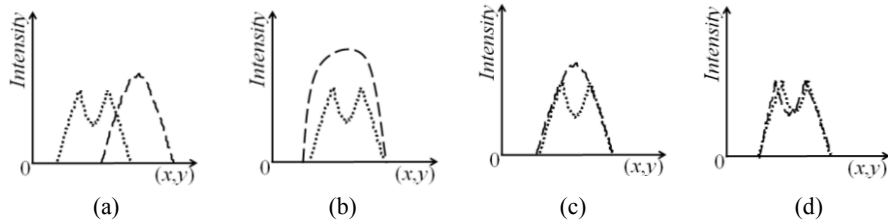


Fig. 6. 2D illustrations of 4 chromosomes (dashed curve) and real-compartment (dotted curve).

more diffusion models representing adjacent spots. The real spots are segmented by drawing the contours of the spot-models.

## 5 Results

Several experiments were conducted in order to evaluate the proposed methods. In this respect, we used four different datasets: (i)  $D_1$ : A set of real microarray images from the Stanford Microarray Database (SMD) [16]- which is publicly available and broadly used, (ii)  $D_2$ : A set of real and synthetic microarray images of the collection of Blekas et al [17] which has already been used for the evaluation of other gridding algorithms, (iii)  $D_3$ : A set of synthetic microarray images of the collection of Lehmußola et al [18] which have already been used for the comparison of various established spot-segmentation techniques for microarray images, and (iv)  $D_4$ : A set of real 2D gel images of the collection of the IIBEAA [19]. The results of the experiments are apposed in the following sections.

### 5.1 Results of the gridding method

The  $D_1$  and  $D_2$  datasets were used in the conducted experiments for the evaluation of the proposed approach. The efficiency of the proposed method was evaluated by means of the statistical analysis described by Blekas et al [17]. More precisely, each microarray spot was classified in one of the following three categories: ‘perfectly’, ‘marginally’ and ‘incorrectly’ gridded. A spot was ‘perfectly’ gridded if the entire spot area was contained inside the equivalent compartment of the grid. A spot was ‘marginally’ or ‘incorrectly’ gridded - respectively - if more or less than 80% of the entire spot area was contained inside the equivalent compartment of the grid.

Using the proposed gridding method, 95.1% of spots were perfectly placed inside the compartment, 4.3% were very nearly gridded, while only 0.6% were gridded incorrectly. It should be pointed out that our gridding method outperforms established techniques, such as the one proposed by Blekas et al, as well as popular software programs such as ScanAlyze and SpotFinder. Fig. 7 depicts the gridding results of a noisy and a rotated microarray sub-image containing several spots of various intensities and sizes. These examples indicate that the effectiveness of the proposed method is not influenced by spot intensities and sizes, neither by rotations and misalignments of the ideal rectangular grid nor by artifacts.

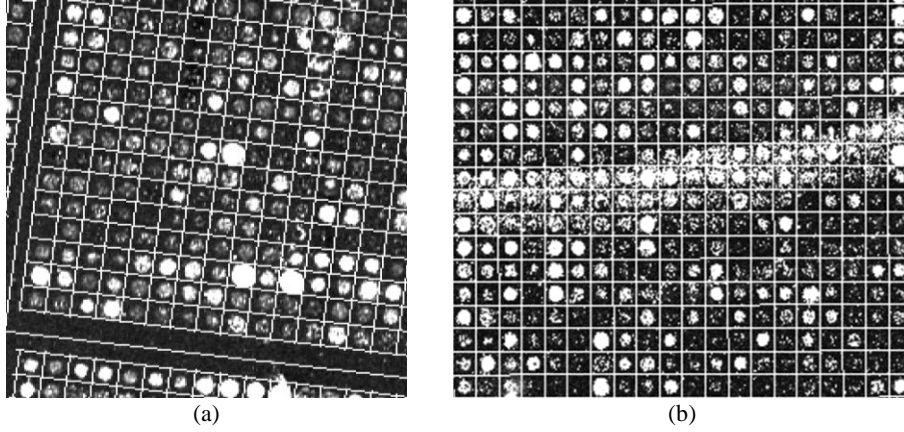


Fig 7. Gridding results of a rotated (a) and noisy (b) microarray sub-image.

## 5.2 Results of the spot-segmentation method for microarray images

The  $D_1$  and  $D_3$  datasets were used in the conducted experiments for the evaluation of the proposed approach. In order to compare objectively the proposed segmentation method with established methods, we used the dataset  $D_3$  of synthetic microarray images and we examined the pixel-level accuracy of our segmentation's method by using the following two measures: The first one is the probability of error  $PE$  and the second one is the discrepancy distance  $D$ .

The comparable results between the proposed method (last row) and other eight established segmentation techniques (first eight rows) – as they are reported by Lehmußola et al – are shown in table I. By comparison, it becomes obvious that the proposed method is radically more successful than the other eight techniques, indicating its high performance. Moreover, it is evident that the proposed method can

**TABLE I**  
**PROPOSED METHOD VS ESTABLISHED TECHNIQUES**  
*COMPARISON ON SYNTHETIC MICROARRAY IMAGES*

Algorithm	Probability of error		Discrepancy distance	
	<u>GQI</u>	<u>LQI</u>	<u>GQI</u>	<u>LQI</u>
Fixed Circle	0.049	0.049	0.027	0.027
Adaptive Circle	0.019	0.192	0.017	0.074
Seeded region growing	0.099	0.114	0.037	0.048
Mann-Whitney	0.165	0.162	0.066	0.074
Hybrid k-means	0.017	0.020	0.016	0.029
Markov random field	0.154	0.053	0.063	0.039
Matarray	0.004	0.031	0.008	0.068
Model-based segmentation	0.094	0.101	0.052	0.067
<b>Proposed method</b>	<b>0.000</b>	<b>0.012</b>	<b>0.000</b>	<b>0.018</b>

optimally segment the spots of good quality images (GQI) while it can very efficiently segment the spots of low quality images (LQI). The significant number of spots which are contained in the used dataset additionally supports these arguments. Indeed, the evaluation of all methods has been statistically calculated in 50000 artificial microarray spots for which the ground truth is given, which means that the correct segmentation result is known.

Fig. 8a illustrates the segmentation result of a microarray block taken from a good-quality synthetic image, while Fig. 8b illustrates the segmentation result of a microarray block taken from a low-quality synthetic image. On these segmentation results, one can observe that the proposed approach has optimally segmented all the microarray spots of Fig.8a and most of the microarray spots of Fig.8b. Moreover, the proposed method has not segmented any spurious spot.

Fig. 9 illustrates four magnified microarray compartments which have been isolated from real microarray blocks obtained from the Stanford Microarray Database. The first two compartments contain a peak-shaped spots, the third one a volcano-shaped spot and the fourth one a doughnut spot. The proposed method has very efficiently segmented the real microarrays spots.

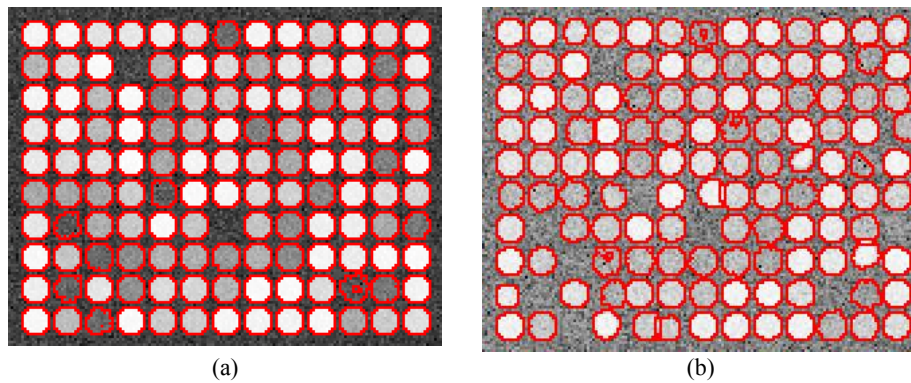


Fig. 8. Spot-segmentation result of a block in a good and low quality Artificial Microarray Image.

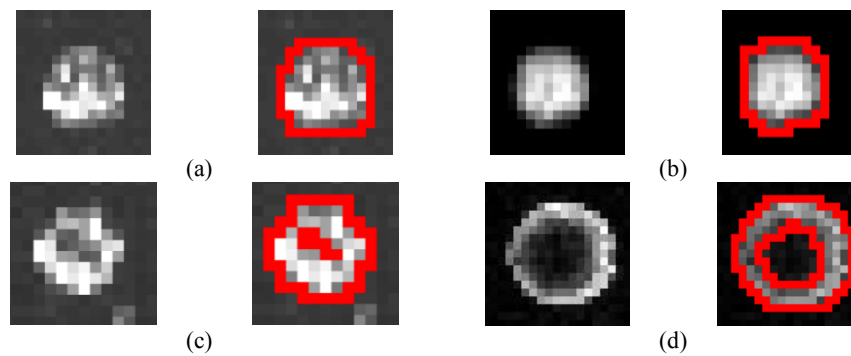


Fig. 9. Spot-segmentation results of several magnified Real Microarray Compartments.

### 5.3 Results of the spot-segmentation method for microarray images

The  $D_4$  dataset was used in the conducted experiments for the evaluation of the proposed approach. An example of spot-segmentation result in a 2D gel image is depicted in Fig. 10. This figure shows that the proposed method did not find any spurious spot whereas Melanie found 6 spurious spots. Both methods detected all the 19 real spots contained in the image. It should be noted that the two points appearing at the upper left corner of Fig. 10a indicate that two spots have been detected, but their boundaries have not been developed enough to capture the whole region of the spot.

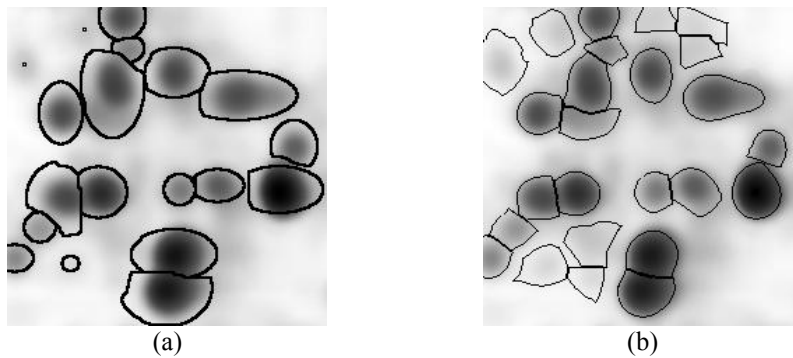


Fig.10. Protein spot detection results of the: (a) proposed approach, (b) Melanie 5 software package.

## 5 Conclusions

In this PhD thesis original image analysis methods have been proposed and applied on real and synthetic biomedical images. The developed ideas lead to satisfying solutions of various issues in image segmentation. Moreover, they bring research one step closer to the objectification of the experimental process since they outperform other well-established techniques and software systems. Last but not least they are fully automatic thus excluding any human intervention that can affect the biological results.

## References

1. E. Zacharia, and D. Maroulis, "An Original Genetic Approach to the Fully-Automatic Gridding of Microarray Images", IEEE Transactions on Medical Imaging, vol.27, no.6, pp. 805-813, June 2008.
2. E. Zacharia, and D. Maroulis, "3D Spot-Modeling for Automatic Segmentation of Microarray Images", IEEE Transactions on NanoBioscience, 2009 (submitted).
3. E. Zacharia, and D. Maroulis, "Advanced evolutionary algorithms for intelligent microarray image analysis", submitted for publication, Handbook of Pattern Recognition and Computer Vision, Chi Chen, World Scientific, 4th edition, 2010 (invitation).

4. D.K. Iakovidis, D. Maroulis, E. Zacharia, and S. Kossida: "A Genetic Approach to Spot Detection in two-Dimensional Gel Electrophoresis images", in Proc. of International Conference on Information Technology in Biomedicine (ITAB), Ioannina, Greece, 2006.
5. E. Zacharia, and D. Maroulis, "An Unsupervised and Fully-Automated Image Analysis Method for cDNA Microarrays", in Proc. of IEEE Computer-Based Medical Systems (CBMS), pp. 389-394, Maribor, Slovenia, 2007.
6. E. Zacharia, and D. Maroulis, "A precise and Automatic Gridding Approach to Noise-Affected and Distorted Microarray Images", in Proc. of IEEE Computer-Based Medical Systems (CBMS), pp. 605-607, Jyvaskyla, Finland, 2008.
7. E. Zacharia, and D. Maroulis, "Microarray Image Gridding via an Evolutionary Algorithm", in Proc. of IEEE Image Processing (ICIP), pp. 1444-1447, San Diego, California, 2008.
8. E. Zacharia, and D. Maroulis, "Microarray Image Analysis based on an Evolutionary Approach", in Proc of the 19th International Conference on Pattern Recognition (ICPR), IAPR, Tampa, Florida, USA, 2008.
9. D. Maroulis, and E. Zacharia, "Microarray Image Segmentation using Spot's Morphological Model", International Conference on Information Technology in Biomedicine (ITAB), November 2009 (accepted).
10. Zacharia, and D. Maroulis, "A genetic approach to cDNA Microarray image Analysis", in Proc. of 11th Panhellenic Conference on Informatics (PCI07), vol. 2, pp. 383-392, Patra, Greece, 2007.
11. D.E. Goldberg, *Genetic Algorithms in Search, Optimization & Machine Learning*, Boston: Addison-Wesley, Reading, 1989, ch. 1.
12. B.L. Miller, and D.E. Goldberg, "Genetic Algorithms, Tournament selection, and the Effects of Noise," *Complex Systems*, vol. 9, no. 3, pp. 193-212, 1995.
13. F. Herrera, M. Lozano, and A.M. Sanchez, "Hybrid crossover operators for real-coded genetic algorithms: An experimental study," *Soft Computing*, vol. 9, no. 4, pp. 280-298, 2005.
14. S.H. Ling, and F.H.F. Leung, "An improved genetic algorithm with average-bound crossover and wavelet mutation operations," *Soft Computing*, vol. 11, no. 1, pp. 7-31, 2007.
15. H. Y. Kim *et al.*, "Characterization and simulation of cDNA microarray spots using a novel mathematical model," *BMC Bioinformatics*, vol. 8, pp. 485-496, March 2007.
16. Stanford Microarray Database. [Online]. Available: <http://genome-www5.stanford.edu/>
17. K. Blekas, N. P. Galatsanos, A. Likas, and I. E. Lagaris, "Mixture Model Analysis of DNA Microarray Images," *IEEE Trans. Medical Imaging*, vol. 24, no. 7, pp. 901-909, July 2005.
18. A. Lehmussola, P. Ruusuvaori, and O. Yli-Harja, "Evaluating the performance of microarray segmentation algorithms," *Bioinformatics*, vol. 22, no. 23, pp. 2910-2917, Oct. 2006.
19. Biomedical Research Foundation (I.B.E.A.A) <http://www.bioacademy.gr/> .